Application of the JPDA-UKF to HFSW Radars for Maritime Situational Awareness

Paolo Braca, Raffaele Grasso, Michele Vespe, Salvatore Maresca and Jochen Horstmann
NATO Undersea Research Centre
La Spezia, Italy
Email: {braca,grasso,vespe,maresca,horstmann}@nurc.nato.int

***Abstract*—At the present day, growing interest is paid to the development of more reliable surveillance systems for maritime situational awareness (MSA). The purpose is to detect, track and classify cooperative and non-cooperative targets. For this reason, great interest is given to low-power/cost High-Frequency Surface-Wave (HFSW) radars as an early-warning tool for over-the-horizon (OTH) applications. However, in HFSW radars there is a trade-off in terms of quality and cost, *i.e.* the radar system exhibits poor azimuth resolution, high non-linearity, and significant false alarm rate. All these aspects reduce tracking performance if not properly addressed. In this context, the Joint Probabilistic Data Association (JPDA) with the Unscented Kalman Filter (UKF) is proposed.**

The tracking algorithm behavior is investigated by a comparison between the tracks generated by two HFSW radars, with overlapped fields of view, and Automatic Identification System (AIS) data. A discussion is provided about the possible effectiveness of HFSW radar fusion strategies.

Preliminary results from a HFSW Radar experiment are reported and discussed.

***Index Terms*—Multi-Target Tracking, HFSW Radar, Maritime Surveillance, Unscented Kalman filter, Data Association, High Clutter Environment**

I. Introduction

In recent years, global political changes have generated significant interest in surveillance applications to combat terrorism, smuggling activities, and illegal immigration. An important theater for these activities is the maritime domain. This has led to a number of national and multinational initiatives in maritime surveillance with the goal of understanding and identifying all coastal and high-seas maritime activities relevant to national security. Ship traffic monitoring continues to present significant challenges (*e.g.* in terms of law enforcement, search and rescue, environmental protection and resource management) and leads to a wide range of requirements. As a fact, in recent years, intensive research activities have been pursued in order to exploit existing sensor systems in support of maritime surveillance. However, this field is far from being fully understood and investigated. In this domain, a variety of sensors can be successfully exploited, but long-range surveillance systems operating on a continuous-time basis are essential. For this reason, great attention has been paid to low-power (50 W on the average) HFSW radars, which are typically exploited for remote sensing applications, in particular, ocean surface current and wave measurements [15]. In addition, they seem to fit well the purpose of ship detection, by virtue of their capability of detecting targets OTH, their continuous and long distance coverage, and target velocity estimation through Doppler analysis. In [14], an overview of the theoretical elements for modeling the backscatter signal is given.

The Wellen Radar (WERA), developed at the University of Hamburg (Germany), is one such system and has proven to be well suited for these purposes. This has been shown by exploiting reports from the Automatic Identification System (AIS) on-board of ships as ground-truth data for assessing ship classification and tracking performance [11], [13].

In [8], the authors address the estimation of detection and localization statistics, proposing a maximum likelihood methodology, which has been applied to HFSW radar data.

It must be considered that the HFSW radar exhibits poor azimuth resolution, high non-linearity, and significant false alarm rate. These issues have been partially solved by a simple Multi-Target Tracking algorithm (MTT), *i.e.* a Nearest Neighbor (NN) data association rule with an $\alpha - \beta$ filter, *e.g.* see [13].

It is well-known that the NN data association rule can be outperformed by more evolved techniques, especially in high clutter environment. The many approaches that exist for solving the data association problem can be broadly characterized as enumerative and non-enumerative. Enumerative approaches, which entail the explicit consideration of data association hypotheses, include Multi-Hypothesis Tracking (MHT), JPDA, $0-1$ integer programming and assignment algorithms, see an overview in [5], [22]. Non-enumerative state estimation approaches include Probabilistic MHT (PMHT), the Symmetric Measurement Equation (SME), event-averaged mean field, and Markov random field methods [5], [22]. Random Finite Set (RFS) theory has also been applied as a non-enumerative approach to MTT [19]. Recent advances in this area have led to implementation of the so-called Probability Hypothesis Density (PHD) filter using Gaussian mixtures and particle approach. Promising results have been obtained in comparison with conventional MHT. An overview of the RFS methodology and PHD filtering is given in [20].

In this work, the application of the JPDA with the UKF [18] is proposed to improve the MTT performance with respect to the NN $\alpha - \beta$ filter, obtaining a good trade-off in terms of performance and complexity/computational load [3].

In radar target tracking the state/measurement equations

Report Documentation Page

Form Approved
OMB No. 0704-0188

1. REPORT DATE	2. REPORT TYPE	3. DATES COVERED
JUL 2012		**00-00-2012 to 00-00-2012**

4. TITLE AND SUBTITLE	5a. CONTRACT NUMBER
Application of the JPDA-UKF to HFSW Radars for Maritime Situational Awareness	5b. GRANT NUMBER
	5c. PROGRAM ELEMENT NUMBER
6. AUTHOR(S)	5d. PROJECT NUMBER
	5e. TASK NUMBER
	5f. WORK UNIT NUMBER
7. PERFORMING ORGANIZATION NAME(S) AND ADDRESS(ES) **NATO Undersea Research Centre,La Spezia, Italy,**	8. PERFORMING ORGANIZATION REPORT NUMBER
9. SPONSORING/MONITORING AGENCY NAME(S) AND ADDRESS(ES)	10. SPONSOR/MONITOR'S ACRONYM(S)
	11. SPONSOR/MONITOR'S REPORT NUMBER(S)

12. DISTRIBUTION/AVAILABILITY STATEMENT
Approved for public release; distribution unlimited

13. SUPPLEMENTARY NOTES
Presented at the 15th International Conference on Information Fusion held in Sinapore on 9-12 July 2012. Sponsored in part by Office of Naval Research and Office of Naval Research Global. U.S. Government or Federal Rights License.

14. ABSTRACT
At the present day, growing interest is paid to the development of more reliable surveillance systems for maritime situational awareness (MSA). The purpose is to detect, track and classify cooperative and non-cooperative targets. For this reason, great interest is given to low-power/cost High-Frequency Surface-Wave (HFSW) radars as an early-warning tool for overthe- horizon (OTH) applications. However, in HFSW radars there is a trade-off in terms of quality and cost, i.e. the radar system exhibits poor azimuth resolution, high non-linearity, and significant false alarm rate. All these aspects reduce tracking performance if not properly addressed. In this context, the Joint Probabilistic Data Association (JPDA) with the Unscented Kalman Filter (UKF) is proposed. The tracking algorithm behavior is investigated by a comparison between the tracks generated by two HFSW radars with overlapped fields of view, and Automatic Identification System (AIS) data. A discussion is provided about the possible effectiveness of HFSW radar fusion strategies. Preliminary results from a HFSW Radar experiment are reported and discussed.

15. SUBJECT TERMS

16. SECURITY CLASSIFICATION OF:			17. LIMITATION OF ABSTRACT	18. NUMBER OF PAGES	19a. NAME OF RESPONSIBLE PERSON
a REPORT **unclassified**	b ABSTRACT **unclassified**	c THIS PAGE **unclassified**	**Same as Report (SAR)**	**8**	

are nonlinear, *e.g.* when the target dynamics are modeled in Cartesian coordinates, while the measurements are directly available in the original sensor coordinates. Furthermore, the HFSW radar (a particular Doppler radar) provides the range rate measurement, which can be used to greatly improve target tracking accuracy. Two methods are commonly used in MTT: tracking in mixed coordinates, *e.g.* see [6], and tracking in Cartesian coordinates, *e.g.* see [9]. The former approach is based on the Extended Kalman Filter (EKF), which suffers from high nonlinearity, that is the case when the range rate measurement is provided. The nonlinear measurement equation is Taylor series expanded around the predicted state to obtain the predicted radar measurements. These approximate expansions, however, can introduce large errors in the posterior mean and covariance of the state estimation, which may sometimes lead to divergence of the filter [10]. Tracking in Cartesian coordinates requires that the measurements in the sensor coordinates are converted to the Cartesian coordinates. The converted measurement error covariance can be quite large for long-range targets [9], which is the case for a HFSW radar.

The UKF addresses the flaws of the EKF by using a deterministic sampling approach. The state distribution is again a Gaussian random vector, but is now represented using a minimal set of carefully chosen sigma points. These sample points capture the true mean and covariance of the Gaussian random vector, and when propagated through the nonlinear measurement equation, they can capture the posterior mean and covariance accurately to the 2nd order [18].

In this paper preliminary results from the NATO Undersea Research Centre (NURC) Battlespace Preparation 2009 (BP09) HFWS Radar experiment, which took place in the Ligurian Sea (Mediterranean Sea) between May and December 2009, are reported and discussed.

The outline is as follows. In Section II some information about the NURC HFSW-radar experiment are provided. The MTT is described in Section III. Experimental results are reported in Section IV. Conclusions and guidelines about future work are drawn in Section V.

II. The HF-Radar experiment

A. The HFSW radar WERA

HFSW radar systems have the capability to detect surface targets well beyond the optical horizon. The operating frequency is in the $3-30$ MHz range (with wavelengths spanning between 100 and 10 m). In this interval, vertically polarized radio waves have also the ability to propagate as surface waves, as long as the surface is conductive due to water salinity.

One such a system is WERA. Its transmitter and receiver are decoupled by using separate locations for the antennas. With this solution, transmitter and receiver can operate simultaneously and illuminate the defined range on a continuous-time basis. Both the transmitter and receiver are made up with quarter-wavelength monopole arrays. The transmitter has a rectangular arrangement, while two different configurations of receiving arrays can be used according to the particular application. A linear receiving antenna array allows it to measure surface current velocities, ocean wave height (spectra) and wind. When the receiver configuration is given by 16 (or 12) line-aligned antennas, the azimuth coverage of the HFSW radar (field of view) is $120°$. WERA system uses frequency modulated continuous wave chirps. Range resolution varies from 0.30 to 1.50 km, depending on the bandwidth of the FM chirp (according to the particular application and spectrum crowding), while Doppler resolution is achieved using CW signals [15].

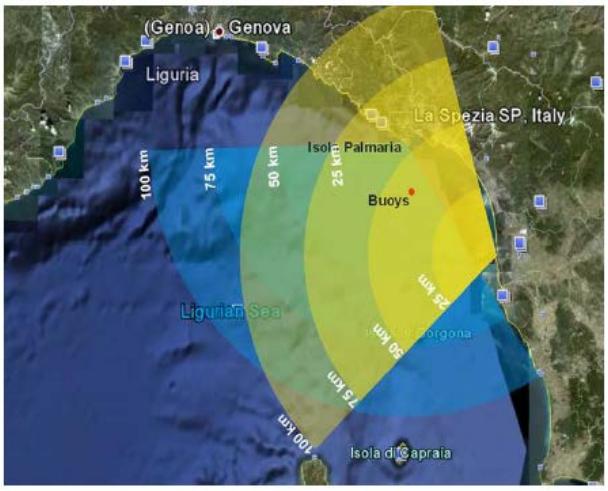

Fig. 1. Map depicting the setup of the two WERA systems in the Ligurian Sea.

B. The AIS system

Ships and vessels exceeding a certain gross tonnage are equipped with AIS transponders for position-reporting, as established by the Safety of Life at Sea (SOLAS) Convention [1]. Ships repeatedly broadcast their name, position and other details for automatic display on nearby ships. While this allows ships to be aware and keep track of other ships in their immediate vicinity, coastal states will also be able to receive, plot and log the data by means of base stations (along the coast. Operating range from shore is expected to depend on the capability and height of the installed base stations. In such a context, most targets are cooperative. Nevertheless a smaller but still significant number is expected to be non-cooperative, or too small to carry an AIS transponder.

C. The experiment setup

Two WERA systems were installed on the Italian coast of the Ligurian Sea, one on Palmaria Island in the Gulf of La Spezia ($44°\ 2'\ 30''$ N, $9°\ 50'\ 36''$ E) and the other one at San Rossore Park near Pisa ($43°\ 40'\ 53''$ N, $10°\ 16'\ 52''$ E), as depicted in Fig. 1. They were operated between May and December 2009 and acquired data on an operational basis to monitor ocean surface currents and waves, and to develop and improve HFSW radar ship detection and tracking algorithms.

The angles with respect to North of the two array installations were $\phi_1 = 296.2°$ and $\phi_2 = 12.0°$, respectively. The experiment started on May 7, 2009 at 14:00:00 UTC. At each

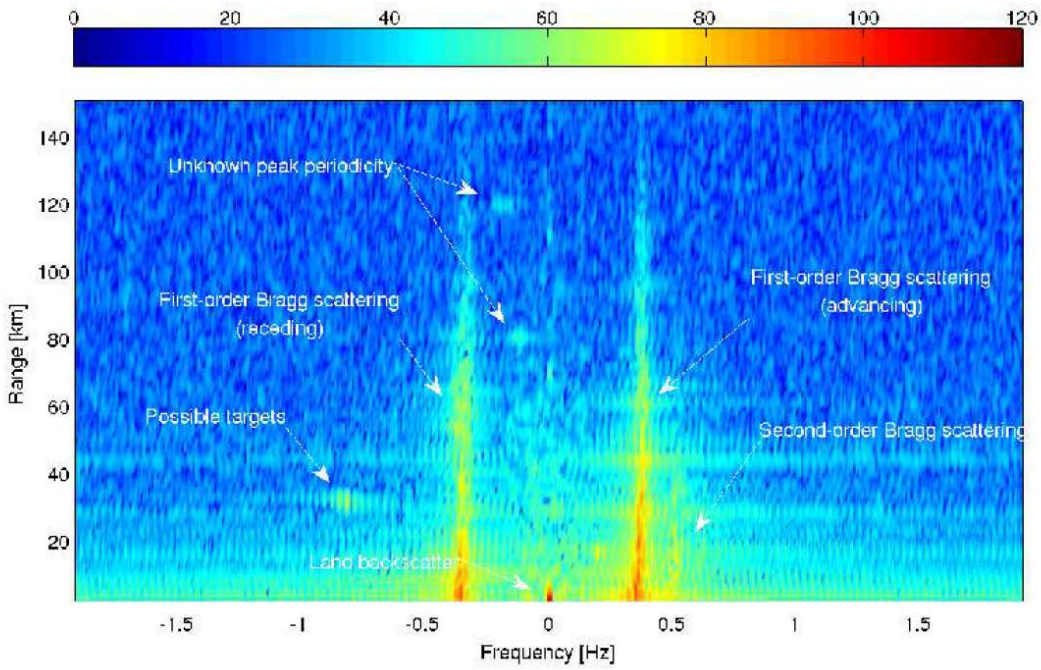

Fig. 2. Example of the HFSW radar range-Doppler map

new hour, WERAs recorded data continuously for 56 minutes and 34 seconds. Such an interval consists of 103 small datasets of 128 samples (33.28s each). Data are recorded by each antenna element in complex samples over all the range cells. The remaining 3 min and 26 s seconds are used to select a new free HFSW channel (between 12.190 and 12.595 MHz) and the available bandwidth according to spectrum crowding. The two systems use the same operating frequency, but the modulating waveforms (sawtooth signal) are orthogonal each other for avoiding coupling interferences. After recording, data from the antennas are beamformed for retrieving azimuth information, then target detection is performed in the Furier domain by the 3D ordered-statistic constant false alarm rate (CFAR) algorithm [11]. Detection is performed on azimuth cells (1° separated) and the detection statistics are evaluated in the range-Doppler space. The coherent processing intervals are composed by 512 samples windows, with an overlap of 75% (*i.e.* a detection occurs every 33.28 s) each. An accurate description can be found in [11], [13].

D. The range-Doppler space

In HFSW radars some common characteristics of the spectrum can be observed and discussed, see *e.g.* [14], [21] and Fig. 2. As far as ship detection is concerned, the contribution of sea clutter is produced by specific spectral components of the surface-height wave-field. The main features are due to first-order Bragg scattering and are generated by those ocean waves of half the radar wavelength and travelling towards and away from the radar site. They correspond to the advancing (positive frequency shift) and receding (negative frequency shift) ground waves. The separation between the two Bragg peaks Δf can be evaluated by [17]

$$\Delta f = 2\sqrt{\frac{g f_c}{\pi c}}, \tag{1}$$

where g is the acceleration due to gravity, c is the speed of light and f_c is the centre-band frequency. In our case, at the HFSW radar operating frequency Δf corresponds to about 0.72 Hz. This phenomenon manifests in the range-Doppler spectrum by means of two lines extending along range, corresponding to the phase-velocities of these scattered ocean waves. However, these frequencies often deviate from the theoretically known values in non-moving waters (*e.g.* underlying surface currents or turbulences due to rocks and cliffs). In addition, second-order Bragg scattering generates side-band contributions in the rang-Doppler spectrum, but are well defined only in the proximity of the radar. Here sea clutter level dominates both targets, noise and interferences. As we move away from the receiving radar, the lines are less defined and the background signal overcomes them. In the very long-range region, sea clutter tends to become a white random process.

Together with sea clutter, especially at near/middle ranges, the contribution of land-scattered echoes around the DC frequencies can be significant. In this case, the two Bragg peaks can undergo a sort of frequency modulation. The evident broadening of the two Bragg frequencies, can be due to rapid changes (*i.e.* turbulences) in the sea waves movement around rock cliffs. In addition, between the two Bragg lines and outside of them, spurious peaks do appear. Some of them are generated by targets. Some of them instead repeat with a certain range-dependent periodicity and are probably due to some unwanted coupling effects with the 50 Hz feeding network. In

the immediately first range cells, a strong contribution around the DC component can be identified. Receiving antennas (with omni-directional pattern) capture signals coming also from cells immediately behind (*i.e.* land), where the back-radiation of the transmitting array is not perfectly zero.

However, sea clutter is not the only type of signal interference we can observe. A variety of interference sources, both natural and man-made, can degrade the reception of ship echoes. The former type usually consists of large returns (horizontal lines), that cover a large portion of the Doppler space. These interferences are principally due to unwanted propagation modes through the ionosphere and/or meteor trails echoes. The second type is instead represented by radio frequency interference (RFI). These returns manifest as vertical lines in the range-Doppler spectrum, and can mask both sea clutter and ship echoes. In fact, they appear at certain Doppler frequency intervals and for all the defined range, almost saturating the whole signal. For overcoming the problem of RFI, an algorithm was proposed by Gurgel *et al.* [16].

III. Multi-target tracking

In this section the MTT technique used to estimate the target trajectories is presented. The following steps need to be described

- Track initiation, maintenance and deletion;
- Association of the radar plot with the existing tracks;
- Filtering, *i.e.* target state update and prediction.

Let us start with describing the target dynamic and measurement model.

A. Target dynamic and measurement model

The target dynamic is defined in Cartesian coordinates

$$\boldsymbol{x}_k = \boldsymbol{f}_k(\boldsymbol{x}_{k-1}, \boldsymbol{w}_k), \tag{2}$$

where $\boldsymbol{f}_k(\cdot)$ is a non-linear function at time k, $\boldsymbol{x}_k$ is the target motion state vector and $\boldsymbol{w}_k$ is the so-called process noise. Given the common motion behavior of large vessels, the constant velocity model [5] is adopted

$$\boldsymbol{x}_k = \boldsymbol{F}_k \boldsymbol{x}_{k-1} + \boldsymbol{\Gamma}_k \boldsymbol{v}_k, \tag{3}$$

where $\boldsymbol{x}_k = [x_k, \dot{x}_k, y_k, \dot{y}_k]^T$, x_k, y_k are the position components along x, y directions, $\dot{x}_k, \dot{y}_k$ are the corresponding velocity components,

$$\boldsymbol{F}_k = \begin{bmatrix} 1 & T_k & 0 & 0 \\ 0 & 1 & 0 & 0 \\ 0 & 0 & 1 & T_k \\ 0 & 0 & 0 & 1 \end{bmatrix}, \boldsymbol{\Gamma}_k = \begin{bmatrix} T_k^2/2 & 0 \\ T_k & 0 \\ 0 & T_k^2/2 \\ 0 & T_k \end{bmatrix},$$

T_k is the current sampling time, $\boldsymbol{v}_k$ takes into account the target acceleration and the unmodeled dynamics, and is assumed to be Gaussian with zero-mean and covariance matrix $\boldsymbol{Q}_k = \sigma_v^2 \boldsymbol{I}$.

Assuming a radar located at the origin of the spherical coordinates, the target-originated measurement equation can be expressed as

$$\boldsymbol{z}_k = \mathbf{h}(\boldsymbol{x}_k) + \boldsymbol{n}_k, \tag{4}$$

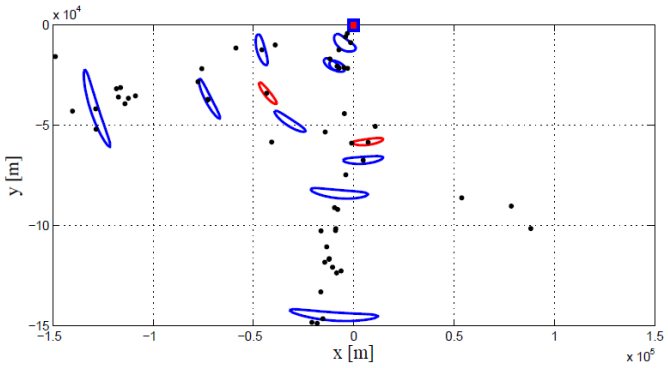

Fig. 3. Validation gates, projected in the Cartesian plane, of confirmed (red line) and preliminary (blue line) tracks, and detections (black dots) at the current time-scan.

the radar measures the target range, bearing (azimuth), and range rate, then the eq. (4) can be recast as follows

$$\begin{aligned} \boldsymbol{z}_k &= \left[z_k^r, z_k^b, z_k^{\dot{r}}\right]^T, \\ \boldsymbol{n}_k &= \left[n_k^r, n_k^b, n_k^{\dot{r}}\right]^T, \\ \mathbf{h}(\boldsymbol{x}_k) &= \left[h_r(\boldsymbol{x}_k), h_b(\boldsymbol{x}_k), h_{\dot{r}}(\boldsymbol{x}_k)\right], \\ h_r(\boldsymbol{x}_k) &= \sqrt{x_k^2 + y_k^2}, \\ h_b(\boldsymbol{x}_k) &= \arctan\left(\frac{y_k}{x_k}\right), \\ h_{\dot{r}}(\boldsymbol{x}_k) &= \frac{x_k \dot{x}_k + y_k \dot{y}_k}{\sqrt{x_k^2 + y_k^2}}, \end{aligned} \tag{5}$$

where $z_k^r, z_k^b, z_k^{\dot{r}}$ are radar measurements of the true target range, bearing, and range rate. The measurement noise vector $\boldsymbol{n}_k$ is assumed to be Gaussian with zero-mean and covariance matrix $\boldsymbol{R}_k$ given by

$$\boldsymbol{R}_k = \begin{bmatrix} \sigma_r^2 & 0 & \rho\sigma_r\sigma_{\dot{r}} \\ 0 & \sigma_b^2 & 0 \\ \rho\sigma_r\sigma_{\dot{r}} & 0 & \sigma_{\dot{r}}^2 \end{bmatrix}.$$

Note that in literature [2], [10] n_k^r,n_k^b,$n_k^{\dot{r}}$ are all assumed to be statistically independent, except that n_k^r and $n_k^{\dot{r}}$ are correlated with a correlation coefficient ρ. Unfortunately no information is present about the parameter ρ in a HFSW radar, and consequently in this work ρ is assumed to be null.

B. Track Management

1) Track formation: The M-of-N rule is used for the track initiation, see details in [4]. If the requirement is satisfied, then the measurement sequence is accepted as a valid track.

The following logic that assumes target position measurements is considered

- Every unassociated measurement is an *initiator*, *i.e.* it yields a *tentative track*.
- At the sampling time following the detection of an initiator, a gate is set up based on the i) assumed maximum (minimum) target dynamic, ii) the measurement noise intensities, *i.e.* if there is a target that gave rise to the

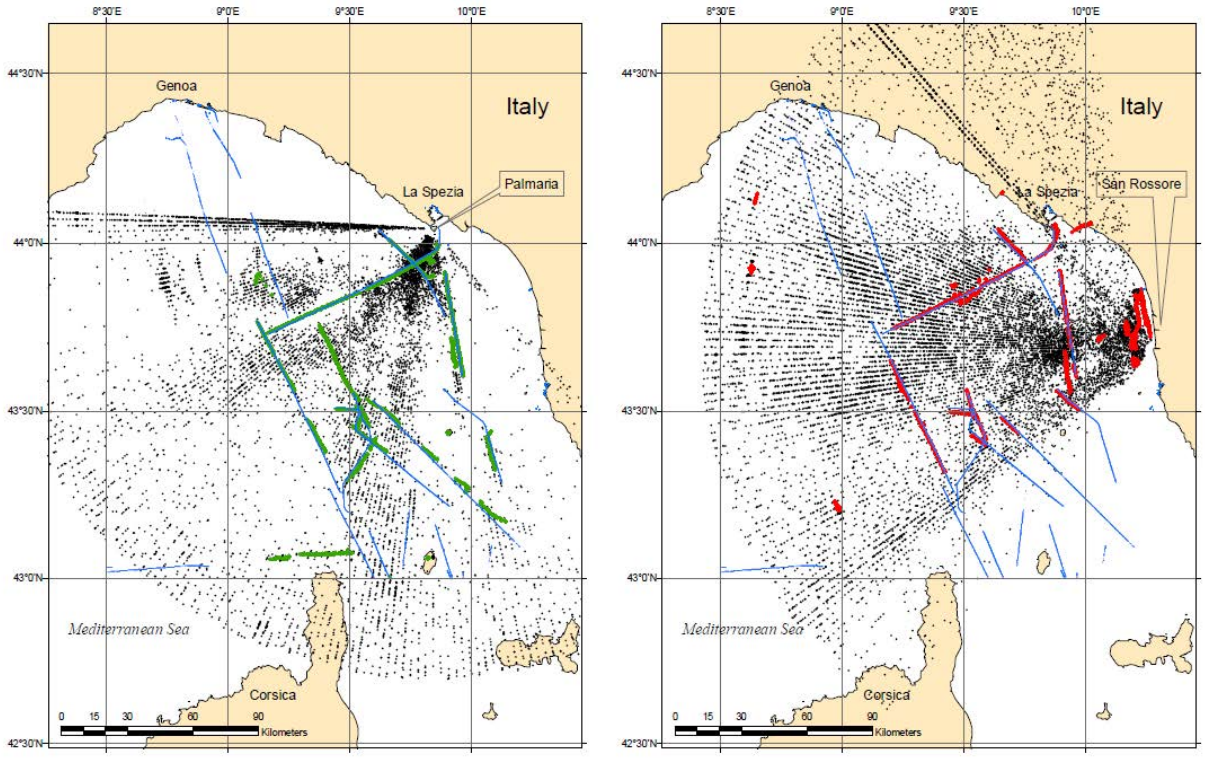

Fig. 4. MTT results of the HFSW system. Left side Palmaria site, target trajectory (green), AIS records (blue) and radar detections (dots). Right side San Rossore site, target trajectory (red), AIS records (blue) and radar detections (dots).

initiator, the possible measurement originated from it in this second scan will fall in the gate with high probability. Following a detection, this track becomes a *preliminary track*. If there is no detection, this track is dropped.

- Since a preliminary track has two measurements, the UKF can be initialized and used to set up a gate for the next sampling time.
- Starting from the third scan a logic of M detections out of N scans is used for the subsequent gates.
- If at the end (scan $N+2$) the logic requirement is satisfied, the track becomes a *confirmed track*. Otherwise it is dropped.

2) Track Termination: A confirmed track is terminated if one of the following event occurs:

- No detections have been validated for the past M^* out of N^* most recent sampling times.
- The target's track uncertainty (state covariance matrix) has grown beyond a certain threshold.
- The target has reached an unfeasible maximum velocity v_{max}.

C. Data Association

The data association rule adopted is the JPDA, which is a Bayesian approach that associates all the validated measurements to the target of interest by probabilistic weights [4], [5]. The JPDA approach can be described by the following steps:

- A validation matrix, that indicates all the possible sources of each measurement is set up. The validation matrix is based on the validation gate of (confirmed and preliminary) targets, indicated by $j = 1, \ldots, J$.
- From the validation matrix, all the feasible joint association events are constructed by the JPDA tracker according to the following two rules $i)$ one measurement must be originated from one target or a false alarm, $ii)$ one target can only generate one measurement at most, with a detection probability P_d.
- The probabilities of these joint events are evaluated according to the following assumptions $i)$ Target-originated measurements are Gaussian distributed around the predicted location of the corresponding targets measurement, $ii)$ false alarms are distributed in the surveillance region according to a Poisson point process model of parameter λ, which represents the clutter density.
- The clutter returns are assumed to be uniformly distributed in the validation regions.
- Marginal (measurement to target) association probabilities are obtained from the joint association probabilities.
- The target states are estimated by averaging the UKF updates by using these marginal probabilities.

D. JPDA-UKF update and prediction

The state update of the j^{th} target $\boldsymbol{x}^j_{k|k}$ is given by [3]

$$\boldsymbol{x}^j_{k|k} = \beta_{0j}\boldsymbol{x}^j_{k|k-1} + \sum_{i=1}^{m_j(k)} \beta_{ij}\boldsymbol{x}^j_{k|k}(i),$$

where $m_j(k)$ is the number of validated measurements for the j^{th} target, $\boldsymbol{x}^j_{k|k-1}$ is the state prediction, $\boldsymbol{x}^j_{k|k}(i)$ is the UKF update using the i^{th} validated measurement, and β_{ij} is the related association probability [4]

$$\begin{aligned} \beta_{0j} &= P\left\{ \text{ no meas. are originated by } j^{th} \text{ targ.} \right\}, \\ \beta_{ij} &= P\left\{ \ i^{th} \text{ meas. is originated by } j^{th} \text{ targ.} \right\}. \end{aligned}$$

The state update covariance is given by [3]

$$\boldsymbol{P}^j_{k|k} = \beta_{0j}\boldsymbol{P}^j_{k|k-1} + \sum_{i=1}^{m_j(k)} \left[\boldsymbol{P}^j_{k|k}(i) + (\boldsymbol{x}^j_{k|k}(i) - \boldsymbol{x}^j_{k|k})(\boldsymbol{x}^j_{k|k}(i) - \boldsymbol{x}^j_{k|k})^T \right] \beta_{ij}. \quad (6)$$

The state prediction $\boldsymbol{x}^j_{k|k-1}$, its covariance $\boldsymbol{P}^j_{k|k-1}$, the predicted targets measurement $\boldsymbol{z}^j_{k|k-1}$ and its covariance $\boldsymbol{S}^j_k$, are provided by the UKF prediction step, see eqs. (8)-(9)-(11)-(12) in Appendix A.

E. Validation gate

Given that the target-originated measurements are Gaussian distributed around the predicted location of the corresponding targets measurement $\boldsymbol{z}^j_{k|k-1}$, the validation gate is defined by the following ellipsoid [5]

$$\mathcal{G}_j(k,\gamma) = \left\{ \boldsymbol{z} : \left(\boldsymbol{z} - \boldsymbol{z}^j_{k|k-1} \right) (\boldsymbol{S}^j_k)^{-1} \left(\boldsymbol{z} - \boldsymbol{z}^j_{k|k-1} \right) < \gamma \right\},$$

with a gate probability determined by the threshold γ. It is interesting to note that in the spherical domain the validation gate has an elliptical shape while, projected into the Cartesian plane $x-y$, has a kind of "banana"-shape, see also comments in [18]. For instance in Fig. 3 validation gates of confirmed and preliminary tracks, in the Cartesian plane, are depicted respectively by red and blue curves, while black dots are the detections at the current time-scan. The banana shape seems to better represent the uncertainty with respect to the classic elliptical shape given that the angular resolution is low and the point in which the gate is centered is located in far-range.

IV. Experiment Results

In this section the MTT has been tested on a subset of the NURC BP09 experiment data set. Data from the Palmaria and San Rossore WERA radars have been processed separately using the CFAR algorithm developed at the University of Hamburg, the detections are then provided to the MTT system described in Section III. Fig. 4 shows the results for 200 radar scans (almost two hours) starting from May 10, 2009 at midnight. In particular, the left and right side pictures depict CFAR detections (black dots) and MTT tracks generated from the radar in Palmaria (green) and San Rossore (red), respectively, with superimposed AIS contacts (blue). In Table I the main values of MTT parameters are also reported.

In Fig. 4 almost $60-70\%$ of AIS tracks are coherent with the radars tracks, *i.e.* AIS tracks belong to the radar track uncertainty regions. Other AIS tracks, up to the final time $k = 200$, are not detected by radars and consequently the related tracks are not present. An interesting aspect is the track fragmentation. It is frequent to observe consecutive missed detections of the same target, in other words the vessel "disappears". This can be due to the decreasing of the radar cross section (*e.g.* different target angulation), or the signal to clutter ratio (*e.g.* vessel is in the Bragg scattering region of the range-Doppler map). However, even if one radar loses a vessel, the other radar can still be able to detect it, as shown in Scenario B in Fig. 5. A possible solution to overcome the fragmentation problem can be optimizing the detector threshold, *i.e.* by increasing the detection probability with a bearable increase of the false alarm rate. Furthermore, a possible solution can be also to adopt an opportune MTT fusion strategy. More details will be provided in the next section.

An interesting result is the presence of high-confidence tracks without AIS confirmation, as depicted in Fig. 5 Scenario A. This aspect has a great relevance for the problem of the AIS spoofing, *i*.e. the HFSW system can detect/track large vessels, independently from the AIS.

A. MTT fusion: a first look

The fusion of data collected by HFSW systems separated by very long baselines enables spatial diversity to improve tracking capabilities, *e.g.* see some preliminary results in [7]. In Scenario B in Fig. 5, where each MTT system leads to different tracks that can be superimposed in order to obtain a more complete traffic picture.

Moreover, illuminating the same region with multiple angles can help overcoming the problems concerning the Doppler shifts and the Radar Cross Section (RCS) of the targets. Since ship detection is here implemented in the frequency domain, missed detections may happen when the vessel Doppler shift falls in the proximity of the most relevant Bragg scattering contributions.

Separated acquisition geometries allow to measure different radial velocity components, yielding a reduction of missed detections and tracks. The aspect diversity also allows the reduction of RCS variability due to the target orientation. This can be severe in the HFSW range, where strong fluctuations from head-on to broadside orientation of the target may occur [12]. As a consequence the setup of two systems can resolve the aforementioned issues. Additional performance limiting factors related to single aspect HFSW systems are represented by shadowing effects, measurement noise, and reduced antenna gain due to non-uniform patterns [13]. All these issues are currently under investigation.

V. Summary

Low-power/cost HFSW radars can be reliable long-range early-warning tools for maritime situational awareness appli-

Parameter	*Value*	*Specification*
T_k	$\approx 33\,\mathrm{s}$	Sampling Period
σ_Q	$5\,10^{-2}\,\frac{\mathrm{m}}{\mathrm{s}^2}$	Process noise par.
σ_r	$350\,\mathrm{m}$	Range measurement std. dev.
σ_b	1°	Bearing measurement std. dev.
$\sigma_{\dot{r}}$	$0.5\,\frac{\mathrm{m}}{\mathrm{s}}$	Range rate measurement std. dev.
P_d	0.5	Detection probability
γ	3.3^2	Gate threshold
$\sigma_{x,y}$	$1\,\mathrm{km}$	Initializing filter const. (pos.)
σ_{v_x,v_y}	$7.5\,\frac{\mathrm{m}}{\mathrm{s}}$	Initializing filter const. (vel.)
λ	$10^{-10}\,\mathrm{m}^{-2}$	Clutter density
v_{max}	$20\,\frac{\mathrm{m}}{\mathrm{s}}$	Maximum velocity
M/N	$5/6$	Track formation logic
M^*/N^*	$4/4$	Track delete logic

TABLE I
PARAMETER VALUES USED IN THE MTT.

cations.

In this paper, preliminary results of the NURC BP09 experimentation (HFSW radar) have been presented and discussed. The radar system exhibits poor azimuth resolution, high non-linearity, and significant false alarm rate. To overcome these limitations, the JPDA-UKF has been proposed. The tracking algorithm behavior has been investigated by a comparison between the tracks generated by radars and Automatic Identification System data. The possible effectiveness of HFSW radars fusion strategies is also commented.

APPENDIX A
UNSCENTED KALMAN FILTER

The adopted tracker filtering is the UKF, which integrates a standard Kalman filter prediction-update iteration with the *Unscented Transform* [18] in order to sequentially estimate the target state eq. (2), given the observation $\boldsymbol{z}_k$, see eq. (4). In our case we concentrate on the j^{th} target, assuming that the i^{th} measurement $\boldsymbol{z}_{i,k}$ is target originated.

UKF prediction

The UKF prediction step starts with the calculation of the sigma point matrix

$$\boldsymbol{\chi}^j_{k-1|k-1} = \left[\boldsymbol{\chi}^j_{k-1|k-1}(0), \ldots, \boldsymbol{\chi}^j_{k-1|k-1}(2n_x)\right],$$

that is given by

$$\begin{aligned}\boldsymbol{\chi}^j_{k-1|k-1} &= \Big[\boldsymbol{x}^j_{k-1|k-1}, \boldsymbol{X}^j_{k-1|k-1} + \widetilde{\boldsymbol{P}}^j_{k-1|k-1}, \\ &\qquad \boldsymbol{X}^j_{k-1|k-1} - \widetilde{\boldsymbol{P}}^j_{k-1|k-1}\Big], \\ \widetilde{\boldsymbol{P}}^j_{k-1|k-1} &= \sqrt{(n_x + \varsigma)\,\boldsymbol{P}^j_{k-1|k-1}}\end{aligned} \tag{7}$$

where ς is a scaling parameter and $\widetilde{\boldsymbol{P}}^j_{k-1|k-1}$ is the Cholesky factorization of the scaled state covariance matrix, $\boldsymbol{X}^j_{k-1|k-1}$ is the $n_x \times n_x$ matrix whose columns are all equal to $\boldsymbol{x}^j_{k-1|k-1}$. The sigma points are propagated through the state transition equation

$$\widetilde{\boldsymbol{\chi}}^j_{k|k-1} = \left[\boldsymbol{f}(\boldsymbol{\chi}^j_{k-1|k-1}(0)), \ldots, \boldsymbol{f}(\boldsymbol{\chi}^j_{k-1|k-1}(2n_x))\right],$$

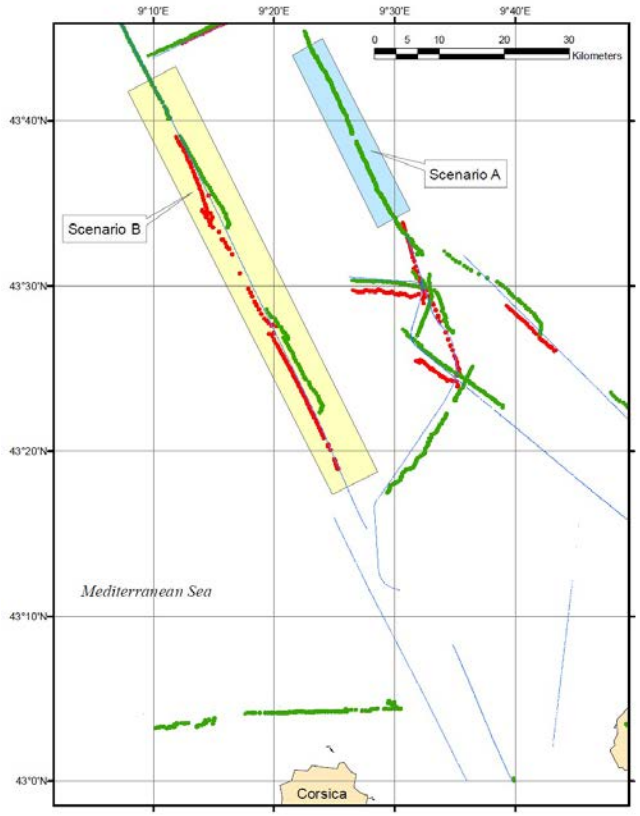

Fig. 5. Target trajectories of Palmaria and San Rossore radars (green and red respectively), AIS records (blue). Scenario A shows a high confidence radar track without its related AIS track. Scenario B shows the potentiality of a track fusion strategy using two HFSW radars.

to predict the state vector by using the unscented weights w_n [18]

$$\boldsymbol{x}^j_{k|k-1} = \sum_{n=0}^{2n_x} w_n \widetilde{\boldsymbol{\chi}}^j_{k|k-1}(n), \tag{8}$$

and computing the prediction state covariance matrix by adding the state noise covariance matrix

$$\begin{aligned}\boldsymbol{P}^j_{k|k-1} = \boldsymbol{Q}_k + \\ \sum_{n=0}^{2n_x} w_n \left(\widetilde{\boldsymbol{\chi}}^j_{k|k-1}(n) - \boldsymbol{x}^j_{k|k-1}\right)\left(\widetilde{\boldsymbol{\chi}}^j_{k|k-1}(n) - \boldsymbol{x}^j_{k|k-1}\right)^T,\end{aligned} \tag{9}$$

where $\boldsymbol{Q}_k$ is state noise covariance matrix. The sigma points are re-drawn to take into account the effect of the state noise process by using the propagated state and state covariance estimates

$$\begin{aligned}\boldsymbol{\chi}^j_{k|k-1} &= \left[\boldsymbol{x}^j_{k|k-1}, \boldsymbol{X}^j_{k|k-1} + \widetilde{\boldsymbol{P}}^j_{k|k-1}, \boldsymbol{X}^j_{k|k-1} - \widetilde{\boldsymbol{P}}^j_{k|k-1}\right], \\ \widetilde{\boldsymbol{P}}^j_{k|k-1} &= \sqrt{(n_x + \varsigma)\,\boldsymbol{P}^j_{k|k-1}}\end{aligned} \tag{10}$$

and successively propagated through the observation equation (4)

$$\boldsymbol{\gamma}^j_{k|k-1} = \left[\mathbf{h}(\boldsymbol{\chi}^j_{k|k-1}(0)), \ldots, \mathbf{h}(\boldsymbol{\chi}^j_{k|k-1}(2n_x))\right],$$

in order to predict the observation vector and its covariance matrix

$$\boldsymbol{z}^j_{k|k-1} = \sum_{n=0}^{2n_x} w_n \boldsymbol{\gamma}^j_{k|k-1}(n), \tag{11}$$

$$\boldsymbol{S}^j_k = \boldsymbol{R}_k + \sum_{n=0}^{2n_x} w_n \left(\boldsymbol{\gamma}^j_{k|k-1}(n) - \boldsymbol{z}^j_{k|k-1}\right)\left(\boldsymbol{\gamma}^j_{k|k-1}(n) - \boldsymbol{z}^j_{k|k-1}\right)^T. \tag{12}$$

UKF update

Upon the reception of the i^{th} measurement $\boldsymbol{z}_k(i)$, and after the calculation of the innovation $\boldsymbol{z}_k(i) - \boldsymbol{z}^j_{k|k-1}$, the state vector and the state covariance matrix predictions are then updated through the standard Kalman filter update step

$$\begin{aligned} \boldsymbol{x}^j_{k|k}(i) &= \boldsymbol{x}^j_{k|k-1} + \boldsymbol{W}^j_k \left(\boldsymbol{z}_k(i) - \boldsymbol{z}^j_{k|k-1}\right) \\ \boldsymbol{P}^j_{k|k} &= \boldsymbol{P}^j_{k|k-1} - \boldsymbol{W}^j_k \boldsymbol{S}^j_k \left(\boldsymbol{W}^j_k\right)^T \end{aligned} \tag{13}$$

where the Kalman filter gain is computed by [18]

$$\begin{aligned} \boldsymbol{W}^j_k = &\sum_{n=0}^{2n_x} w_n \left(\boldsymbol{\chi}^j_{k|k-1}(n) - \boldsymbol{x}^j_{k|k-1}\right) \\ &\cdot \left(\boldsymbol{\gamma}^j_{k|k-1}(n) - \boldsymbol{z}^j_{k|k-1}\right)^T \left(\boldsymbol{S}^j_k\right)^{-1}. \end{aligned} \tag{14}$$

REFERENCES

[1] *Safety of Life at Sea (SOLAS) Convention*. Chapter V, Regulation 19.

[2] Y. Bar-Shalom, "Negative correlation and optimal tracking with Doppler measurements," *IEEE Trans. Aerosp. Electron. Syst.*, vol. 37, no. 3, pp. 1117–1120, Aug. 2001.

[3] Y. Bar-Shalom, F. Daum, and J. Huang, "The probabilistic data association filter," *IEEE Control Syst. Mag.*, vol. 29, no. 6, pp. 82–100, Dec. 2009.

[4] Y. Bar-Shalom and X. Rong Li, *Multitarget-Multisensor Tracking: Principles and Techniques*. Storrs, CT: YBS Publishing, 1995.

[5] Y. Bar-Shalom, P. Willett, and X. Tian, *Tracking and Data Fusion: A Handbook of Algorithm*. Storrs, CT: YBS Publishing, 2011.

[6] D. Bizup and D. Brown, "The over-extended Kalman filter-don't use it!" in *Proc. of the 6^{th} International Conference on Information Fusion (FUSION)*, Cairns, Queensland, Australia, July 2003, pp. 40–46.

[7] P. Braca, M. Vespe, S. Maresca, and J. Horstmann, "A novel approach to high frequency radar ship tracking exploiting aspect diversity," in *Proc. of the IEEE International Geoscince and Remote Sensing Symposium (IGARSS)*, Munich, 2012.

[8] C. Carthel, S. Coraluppi, P. Willett, M. Maratea, and A. Maguer, "Maximum likelihood approach to HF radar performance characterization," in *Proc. of the 12^{th} International Conference on Information Fusion (FUSION)*, Seattle, U.S.A., Jul. 2009, pp. 1–8.

[9] Z. Duan, C. Han, and X. Rong Li, "Sequential nonlinear tracking filter with range-rate measurements in spherical coordinates," in *Proc. of the 7^{th} International Conference on Information Fusion (FUSION)*, Stockholm, Sweden, June 2004, pp. 599–605.

[10] Z. Duan, X. Rong Li, C. Han, and H. Zhu, "Sequential unscented Kalman filter for radar target tracking with range rate measurements," in *Proc. of the 8^{th} International Conference on Information Fusion (FUSION)*, Philadelphia, PA, U.S.A., July 2005, pp. 130–137.

[11] A. Dzvonkovskaya, K.-W. Gurgel, H. Rohling, and T. Schlick, "Low power high frequency surface wave radar application for ship detection and tracking," in *Proc. of the IEEE Radar Conference*, Vilnius, Lithuania, 2010.

[12] A. Dzvonkovskaya and H. Rohling, "Cargo ship RCS estimation based on HF radar measurements," in *Proc. of the International Radar Symposium (IRS)*, Adelaide, Australia, Jun. 2010.

[13] ——, "HF radar performance analysis based on AIS ship information," in *Proc. of the IEEE Radar Conference*, Washington, USA, 2010.

[14] S. Grosdidier, A. Baussard, and A. Khenchaf, "HFSW radar model: Simulation and measurement," *IEEE Trans. Geosci. Remote Sens.*, vol. 48, no. 9, pp. 3539–3549, Sep. 2010.

[15] K.-W. Gurgel, G. Antonischki, H.-H. Essen, and T. Schlick, "Wellen radar (WERA), a new ground-wave based HF radar for ocean remote sensing," *Coastal Engineering*, vol. 37, no. 3, pp. 219–234, Aug. 1999.

[16] K.-W. Gurgel, Y. Barbin, and T. Schlick, "Radio frequency interference suppression techniques in FMCW modulated HF radars," in *Proc. of Oceans 2007 Europe*, Aberdeen, Scotland, 2007.

[17] J. Headrick and M. Skolnik, "Over-the-horizon radar in the HF band," *Proc. IEEE*, vol. 62, no. 6, pp. 664–673, Jun. 1974.

[18] S. J. Julier and J. K. Uhlmann, "Unscented filtering and nonlinear estimation," *Proc. IEEE*, vol. 92, no. 3, pp. 401–422, Mar. 2004.

[19] R. Mahler, "Multitarget Bayes filtering via first-order multitarget moments," *IEEE Trans. Aerosp. Electron. Syst.*, vol. 39, no. 4, pp. 1152–1178, Jan. 2003.

[20] ——, *Statistical Multisource-Multitarget Information Fusion*. Artech House, 2007.

[21] S. Maresca, M. Greco, F. Gini, R. Grasso, S. Coraluppi, and N. Thomas, "The HF surface wave radar WERA. part II: Spectral analysis of recorded data," in *Proc. of the IEEE Radar Conference*, Washington, USA, 2010.

[22] G. W. Pulford, "Taxonomy of multiple target tracking methods," *Proc. of IEE Radar Sonar Navig.*, vol. 152, no. 5, pp. 291–304, Oct. 2005.